International Forum on Aeroelasticity and Structural Dynamics
IFASD 2024
17-21 June 2024, The Hague, The Netherlands

AN INTEGRATED STATIC/DYNAMIC AEROTHERMOELASTIC ANALYSIS FRAMEWORK FOR FUNCTIONALLY GRADED STRUCTURES IN HYPERSONIC VEHICLES

Li Chang[1], Wan Zhiqiang[1], Wang Xiaozhe[2] and Yang Chao[1]

[1] School of Aeronautic Science and Engineering, Beihang University, Beijing 100191, China
[2] Institute of Unmanned System, Beihang University, Beijing 100191, China

Keywords: aerothermoelasticity, hypersonic vehicles, aeroelasticity, functionally graded materials

Abstract: Hypersonic vehicles are susceptible to considerable aerodynamic heating and noticeable aerothermoelastic effects during flight due to their high speeds. Functionally graded materials (FGMs), which enable continuous changes in material properties by varying the ratio of two or more materials, provide both thermal protection and load-bearing capabilities, and usually used in thermal protection structures for hypersonic vehicles. This paper establishes an integrated static/dynamic aerothermoelastic analysis framework for FG structures in hypersonic vehicles. This paper presents the integrated static/dynamic aerothermoelastic analysis of a small aspect ratio hypersonic wing with FGM as the skin. The static aerothermoelastic response and flutter characteristics are efficiently obtained during the flight through the framework. Furthermore, the phenomenon of a sudden change in flutter speed with time was also observed.

1 INTRODUCTION

Hypersonic vehicles, defined as those with a flight Mach number greater than 5, have emerged as a crucial area of interest in aerospace applications due to their high flight speed, robust defence capability and extended flight range. A number of hypersonic vehicles have been or are being devised in recent years, including the X-43A, X-51A and SR-72. However, there are considerable technical challenges for hypersonic vehicles, such as the need for more robust aerodynamic computation methods, effective aeroelastic analysis under the heating environment, panel flutter and more complicated coupling of heat, aerodynamic, structure, thrust and other fields [1]. A considerable quantity of aerodynamic heat is generated during flight due to the substantial air friction. This results in a complex coupling effect with the structure, which causes the aerothermoelastic behaviors.

There has been a considerable amount of research conducted in recent years on the subject of aerothermoelasticity. Some of them focused on the panel flutter. Schoneman [2] proposed an aerothermoelastic framework based on the concept of perturbation about a quasi-static solution to analyze dynamic aeroelastic response in the vicinity of each solution point and used it to analyze the flutter and postflutter response of curved panels. Quan [3] investigated the post-flutter aerothermoelastic behaviors of the hypersonic skin panels by using the integrated aerothermoelastic analysis framework. Venegas and Huang [4] presented a physics-infused

reduced order modeling methodology of hypersonic aerothermal loads for aerothermoelastic analysis. Xie [5] investigated the effect of thermal protection system size on aerothermoelastic stability of the hypersonic panel. Vidanović [6] conducted a multidisciplinary shape optimization of missile fin configuration under the aerodynamic heating.

Due to the severe aerodynamic heating that occurs in hypersonic vehicles, it is often necessary to implement a thermal protective layer on the surface to safeguard the structures and devices inside the vehicle. The thermal insulation layer and the structural layer are composed of disparate materials with distinct mechanical characteristics. This can result in the formation of stress concentrations, delamination, peeling, and other interfacial phenomena, which impair the structural integrity and safety of the vehicle. In order to avoid these, Japanese researchers proposed the concept of functionally graded materials (FGMs), which involve the continuous alteration of the material properties of two or more materials through varying their compositions and structures. This ensures that there is no discernible interface or structural mutation. There are also numerous studies on the panel flutter of functionally graded (FG) plates. Praveen and Reddy [7] employed a finite element approach that considered shear strain to assess both the static and dynamic responses of ceramic-metal FG plates under different transient temperature fields. Khalafi [8] conducted a panel flutter analysis of cracked functionally graded plates in yawed supersonic flow with thermal effects. Xia [9] constructed a three-node triangular element based on Mindlin plate theory and used a multinode approach to construct a reduced-order model to analyze the nonlinear flutter response of preheated FG plates.

However, in the current researches on the structure of FGMs, the majority of studies are focused on the fundamental research on plates, with minimal investigation into their application in actual structures in hypersonic vehicles. Due to the heat-resistant and load-bearing characteristics of FGM structures in hypersonic vehicles, and that the structural properties of FGMs are significantly affected by thermal loads, it can be concluded that their dynamic aerothermoelastic performances are significantly affected by temperature. Furthermore, thermal flutter analysis and static aerothermoelastic analysis, as important issues in hypersonic vehicles, are usually studied separately from each other.

Therefore, based on the characteristics that FGMs are significantly affected with thermal loading, this paper proposes an integrated static/dynamic aerothermoelastic analysis framework for functionally graded structures in hypersonic vehicles. The framework is capable of analyzing both the flutter and the static aerothermoelastic behaviors simultaneously. It employs a two-way coupling strategy and a loose coupling approach in its computational method. It performs aerodynamic analysis, aerodynamic thermal analysis, and heat conduction analysis, and heated structural analysis, respectively. The flutter characteristics and responses through the flight can be acquired, thereby facilitating rapid aerothermoelastic analysis, which provides the foundation for the design of hypersonic vehicles.

2 METHODS

Aerothermoelasticity is a highly intricate physical phenomenon that encompasses a multitude of disciplines, including aerodynamics, structural mechanics, and heat transfer theroies, among others. This section introduces the modelling method of FGM, the aerodynamic analysis method, the aerodynamic heating analysis method, and the flutter analysis method, respectively. Furthermore, It also presents the integrated static/dynamic aerothermoelastic analysis framework for functionally graded structures in hypersonic vehicles proposed in this paper.

2.1 Modeling method for FGM

In contrast to the properties of conventional homogeneous materials, the characteristics of FGMs are subject to variation due to their composition comprising a blend of two components. Several models were established to compute the properties of FGM, such as Voigt model, Reuss model, and Mori-Tanaka model. Among these models, Voigt model characterises the properties of the two materials according to the weighted sum of the volume ratios of the local properties. This model is widely used by researchers due to the simplicity of its characterisation, and is also employed in this paper as shown in the following equation.

$$P(z) = P_{\mathrm{m}}\left(1 - V_{\mathrm{c}}\right) + P_{\mathrm{c}}V_{\mathrm{c}} \tag{1}$$

where $P(z)$, P_{c}, and P_{m} express the properties of the FGM, ceramic and metal, respectively. The subscripts c, m and cm denote the properties of the ceramic and metal and the difference between the ceramic and metal, that is,

$$P_{\mathrm{cm}} = P_{\mathrm{c}} - P_{\mathrm{m}} \tag{2}$$

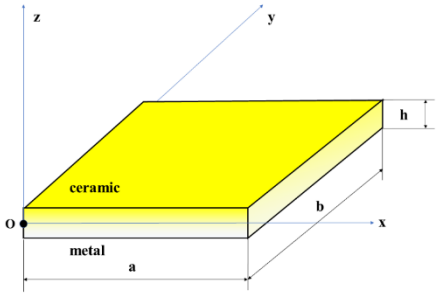

Fig. 1 Coordinate system and geometry of the FG plates.

The FG plate coordinates are presented in Fig. 1. The airflow is assumed to be in the x-direction, and the z coordinate is measured from the mid-plane of the plates. The relationship between the ceramic volume ratio, V_{c} and the z-coordinate can be expressed as follows

$$V_{\mathrm{c}} = \left(\frac{1}{2} + \frac{z}{h}\right)^{k} \tag{3}$$

where k is the volume fraction index of the FGM.

Therefore, for FG plates, the material properties vary according to location in the thickness direction as follows:

$$P(z) = P_m + P_{cm}\left(\frac{1}{2} + \frac{z}{h}\right)^{k} \tag{4}$$

In addition, temperature influences FGMs by altering the material properties and can significantly affect the structure. This phenomenon can be described as the correlation between material properties and an increase in environment temperature, where P_0, P_{-1}, P_1, P_2, and P_3 denote the coefficients of properties and the subscript i denotes the constituent material, such as ‘m’ for metal and ‘c’ for ceramic:

$$P_i(T) = P_0\left(P_{-1}T^{-1} + 1 + P_1T + P_2T^2 + P_3T^3\right) \tag{5}$$

2.2 Aerodynamic analysis method

This paper adapts the local piston theory as the aerodynamic analysis method. The piston theory proposed by Lighthill compares the perturbation of the airflow on the airfoil surface of a supersonic airflow to the perturbation of a piston motion on an infinitely long cylinder, which is convenient for obtaining the aerodynamic force. It is also widely used in the aerodynamic analysis for supersonic and hypersonic wings. The third-order form of the local piston theory can be expressed as follows:

$$C_p(x,t) = \frac{2}{Ma_{local}{}^2}\left[\frac{v_n}{a_{local}} + \frac{\gamma+1}{4}\left(\frac{v_n}{a_{local}}\right)^2 + \frac{\gamma+1}{12}\left(\frac{v_n}{a_{local}}\right)^3\right] \tag{6}$$

where C_p is the pressure coefficient, v_n is the vertical velocity, γ is the gas heat capacity ratio, and Ma_{local} and a_{local} denotes the local Mach number and the local sound speed.

The local parameters in the local piston theory are acquired by the shock/expansion theory in this paper. The shock/expansion theory is an analytical method in two dimensions (2D) when hypersonic airflow passes through a wedge. The method computes the air parameter ratios before and after the oblique shock wave or expansion wave, after computing the relationship between the oblique shock angle and the wedge angle, as follows:

$$\tan\theta = 2\cot\beta\frac{Ma_\infty^2\sin^2\beta - 1}{Ma_\infty^2\left(\gamma + \cos 2\beta\right) + 2} \tag{7}$$

2.3 Aerodynamic heating analysis method

This paper employs Eckert's reference temperature methodology to compute the local flow parameters in the vicinity of the boundary layer between the surface and compressible flow, assuming a reference temperature in the incompressible flow. The results obtained by this method can be applied to compressible flow, provided that the solution for incompressible flow is known. The relationship between the two temperature types is illustrated as follows:

$$T^* = 0.5T_w + 0.22T_r + 0.28T_e \tag{8}$$

where T_{w} is the wall temperature, T_{r} is the recovery tempertature, and T_{e} is the environment temperature.

The Blasius solution allows us to calculate the friction stress based on local flow parameters solved in Eq. (7). Once the reference temperature and friction stress have been obtained, this paper employs the Reynolds analogy method to establish the relationship between the convective heat transfer coefficient and friction stress, as shown in Eq. (8).

$$St^* = \frac{C_f^*}{2\,\mathrm{Pr}^{\frac{2}{3}}} \tag{9}$$

In accordance with the parameters set forth in Eq. (8), the heat flux resulting from convection and radiation can be calculated using Eq. (9) and Eq. (10).

$$Q_{conv} = \rho u C_p \left(T_r - T_w\right) St^* \tag{10}$$

$$Q_{rad} = \sigma\varepsilon\left(T_w^4 - T_\infty^4\right) \tag{11}$$

2.4 Flutter analysis method

There are several typical flutter analysis methods, such as the k-method proposed by Theodorsen by introducing the aerodynamics into a vibration analysis as complex inertial terms and the flutter analysis became a vibration analysis requiring complex arithmetic. Pk-method introduces the aerodynamic loads into the equations of motion as frequency dependent stiffness and damping terms. The pk-method is frequently employed by researchers due to its greater practicality and the direct correlation between the results and the velocity values. This paper utilizes the pk method, as shown in the following equation.

$$\left[\mathbf{M}p^2 + \left(\mathbf{B} - \frac{1}{4k}\rho c V \mathbf{Q^I}\right)p + \left(\mathbf{K} - \frac{1}{2}\rho V^2 \mathbf{Q^R}\right)\right]\mathbf{u} = 0 \tag{12}$$

where **M, B, K, $\mathbf{Q^I}$, $\mathbf{Q^R}$**, and **u** denote the modal mass matrix, the modal damping matrix, the modal stiffness matrix, the imaginary part of the modal aerodynamic force matrix, the real part of the modal aerodynamic force matrix, and the modal amplitude vector, respectively. V is the velocity, c is the reference chord length, g is the artificial structural damping, and ω is the circular frequency. p is the eigenvalue, which can be expressed by Eq. (12), and k is the reduced frequency, which can be expressed by Eq. (13).

$$p = \omega\left(\frac{g}{2} + i\right) \tag{13}$$

$$k = \frac{\omega c}{2V} \tag{14}$$

The flutter characteristics can be obtained by solving the generalized eigenvalue problems by iteration. When the reduced order is specified to be as a series of numbers, the remaining parameters such as the structural damping and the frequency can be obtained. Since the structural damping is added to maintain the equilibrium of the system artificially, when the structural damping becomes into a positive value, and meantime, the frequencies of two orders become close to each other, the flutter occurs.

2.5 Static/dynamic aerothermoelastic analysis framework

Aiming at the characteristics of FGMs that are sensitive to thermal loads and the separation of thermal flutter analysis and static aerothermoelastic analysis for time-domain advancement during the flight history in previous studies, this paper proposes an integrated static/dynamic aerothermoelastic analysis framework for functionally graded structures in hypersonic vehicles.

The analysis framework is divided into two main parts. The static aerothermoelastic analysis module constitutes the framework's principal component. Through the coupled aerodynamic/structural/thermal analysis, the framework enables the investigation of the changes in aerodynamic pressure, heat flow, temperature field and structural properties that occur during the flight history. The thermal flutter analysis module, in contrast, analyses the aeroelastic stability problem under different temperature fields at different moments during the flight.

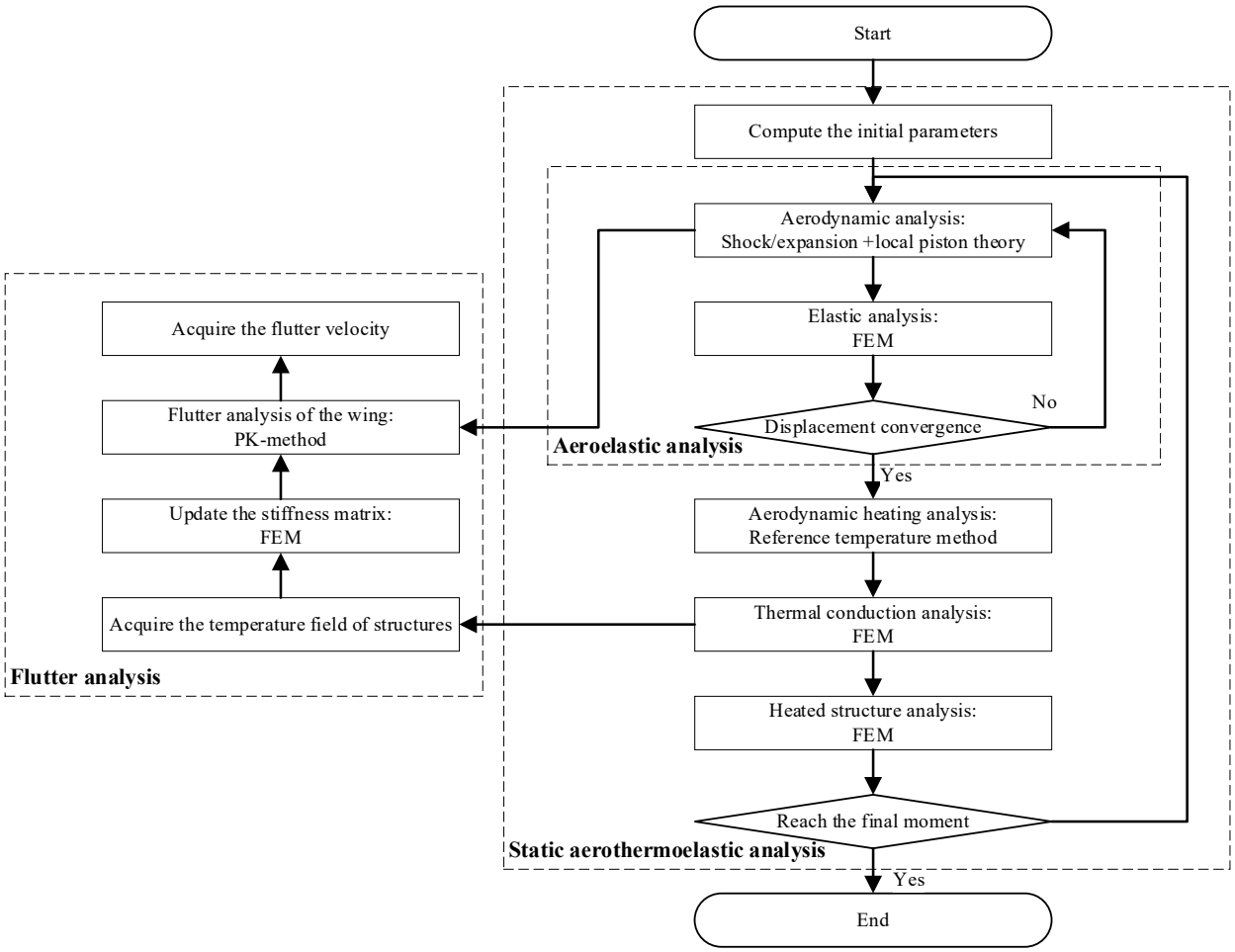

Fig. 2 The flowchart of the integrated static/dynamic aerothermoelastic analysis framework

The analysis process can be divided into the following steps:

1) Calculate the initial parameters of the model. These include initial airflow parameters, initial structural parameters, and initial temperature parameters.

2) Conduct the aerodynamic analysis. The aerodynamic forces were derived from the local piston theory, and the local flow parameters were obtained using the classical shock/expansion theory.

3) Conduct the structural static analysis. The aerodynamic forces obtained from the aerodynamic analyses were interpolated to the structural nodes, and the static analyses were carried out using the finite element method (FEM) to calculate the structural displacements.

4) Conduct the aeroelastic iteration until the convergence of displacement. The structural deformation is interpolated to the aerodynamic surface, and then the aerodynamic force is interpolated to the structural nodes. This iteration is repeated between the structure and the aerodynamics until the displacement difference reaches a predetermined value, thus achieving the aeroelastic convergence.

5) Calculate the aerodynamic heat flux. A two-way coupled analysis is employed to calculate the surface heat flux utilising the reference temperature method, based on the airflow parameters that have been altered by the aeroelastic deformation.

6) Conduct the heat conduciton anlysis. The convective and radiant heat flow applied to the surface of the finite element of the structure is analysed by transient heat conduction in order to obtain the temperature field inside the structure.

7) Conduct the heated structure analysis. The calculation of the thermal deformation of a structure subjected to a thermal loading state, incorporating both the effects of thermal expansion of the structure and thermal degradation of the material properties.

8) Conduct the static aerothermoelastic iteration until the specified moment.The thermal deformation obtained from the heated structure analysis is superimposed on the aeroelastic deformation, and the iterative analysis continues for the next aerothermoelastic time step until the specified final time is reached.

9) Extract the temperature field of the structure. The temperature field at each moment during the flight is extracted from the temperature field at the final moment obtained from the heat conduction analysis.

10) Update the stiffness matrix. The updated stiffness matrix is derived by calculating the updated temperature field, which incorporates thermal expansion and material property changes with temperature, for flutter calculations.

11) Conduct the flutter analysis. The updated stiffness matrix and aerodynamic surfaces were interpolated in order to perform a flutter analysis using the pk-method.

12) Plot V-g curves and V-f curves. The damping ratio and frequency at different reduced frequencies (velocities) can be obtained by the pk-method, which is extracted to plot V-g curves and V-f curves as characteristic curves of flutter.

13) Extract the flutter speed. By the basic principle of the pk-method, a V-g curve crossing the transverse axis from below means that flutter occurs. This enables the extraction of the flutter speed.

3 RESULTS

In this section, the analysis framework proposed by this paper is applied to a typical small aspect ratio wing with a skin made of FGM, which provides both thermal protection and load bearing. The integrated static/dynamic aerothermoelastic analysis is carried out, and the static aerothermoelastic response and thermal flutter of the FGM-containing structure in a hypersonic vehicle during the flight are also analyzed. The relationships between the aeroelastic deformation, thermal deformation, temperature, pressure, heat flux, flutter speed and other physical quantities of the wing at different moments are obtained.

3.1 Model description

The object of analysis is a typical small aspect ratio wing, the geometry of which is shown in Fig. 3. FGMs are used on the skin of the wing and modelled by means of finite element discretization, in this section the skin of the wing is divided into 5 layers to simulate the variation of the FGM properties along the thickness direction, with the volume fraction index chosen to be 1. The material properties of each layer element are assigned using the material properties of the midface of the element in that layer, as shown in Fig. 4. FGM is used as the skin of the wing and The FEM model contains the 1702 shell elements made of Ti-6Al-4V inside the wing and 4320 solid

elements made of Ti-6Al-4V/ZrO_2 FGM in the skin of the wing, as shown in Fig. 5. The material properties of FGM are shown in Table 1.

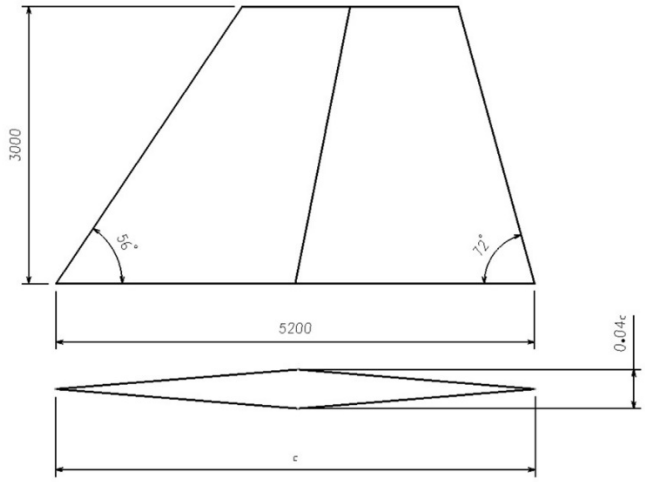

Fig. 3 The geometry of the wing

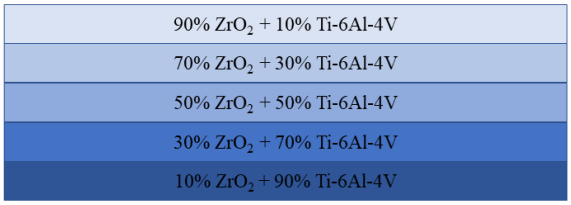

Fig. 4 Schematic of FGM finite element discretization

Table 1. Material properties of FGM

	Material	P_0	P_{-1}	P_1	P_2	P_3
E (Pa)	Ti-6Al-4V	122.70E9	0	-4.605E-4	0	0
	ZrO_2	132.20E9	0	-3.805E-4	-6.127E-8	0
α	Ti-6Al-4V	7.4300E-6	0	7.483E-4	-3.621E-7	0
	ZrO_2	13.300E-6	0	-1.421E-3	9.549E-7	0
ρ (kg/m^3)	Ti-6Al-4V	4429	0	0	0	0
	ZrO_2	3000	0	0	0	0
λ (W/(m·K))	Ti-6Al-4V	7.82	0	0	0	0
	ZrO_2	1.8	0	0	0	0

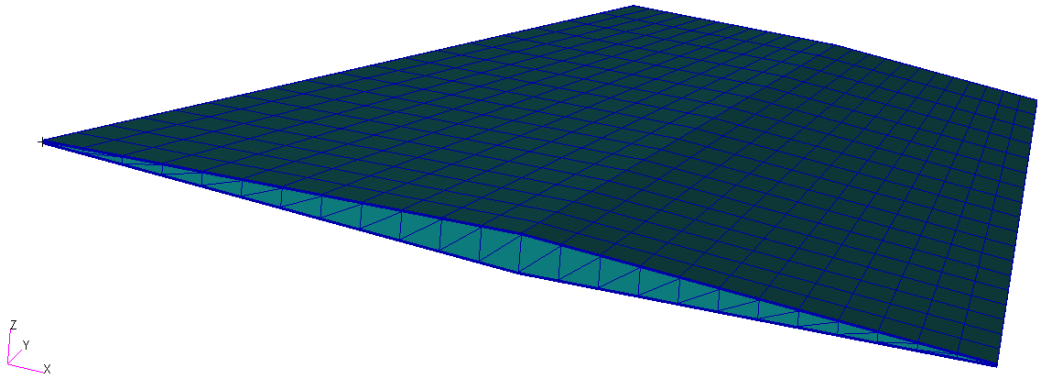

Fig. 5 FEM modeling of the wing

This section analyses the aerothermoelastic characteristics of the cruise phase of this small aspect ratio wing, using flight conditions of Mach number 5, angle of attack 2°, flight time 600 seconds and a step size of 1 second for the thermal analysis.

3.2 Static aerothermoelastic characteristics

Firstly, the relationship between the static aerothermoelastic response over time and the flight path in hypersonic airflow is investigated. Figure 6 illustrates the temporal variation of the maximum aeroelastic deformation and the maximum thermal deformation. The maximum thermal deformation increases rapidly with time, reaching a peak value of 21.36 mm at 225 s, which is almost twice the value of the aeroelastic deformation. Thereafter, it decreases gradually. However, the maximum aeroelastic deformation increases with time. This is due to the gradual penetration of heat into the structure over time. Initially, the temperature outside the structure increases, resulting in a larger thermal deformation. In the subsequent stage, the temperature inside the structure rises, while the temperature difference between the internal and external temperatures of the structure decreases. Consequently, the maximum thermal deformation declines, while the overall stiffness of the structure declines and the aeroelastic deformation increases.

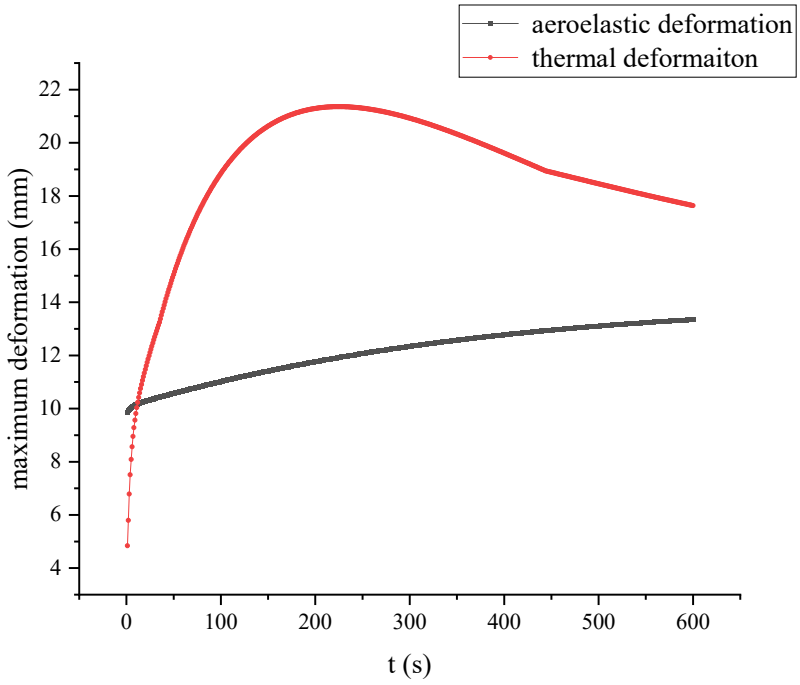

Fig. 6 The variation of the maximum deformation over time

For brevity, this section only shows the change in temperature distribution over time. The temperature distributions of the upper and lower surface at different moments including at t=2 s, t=200 s, t=400 s, and t=600 s are shown in Fig. 7-Fig. 10, respectively. In the initial stage, the temperature distribution partitions roughly coincide with the four regions of the diamond-shaped wing, as the aerodynamic surfaces have not yet deformed in this stage, and the local airflow parameters are determined by the shock/expansion theory, which can be divided into four regions. As time progresses, the temperature continues to increase, with the external temperature remaining

relatively unchanged at the end stage. In contrast, the internal temperature rises significantly. In the temperature distribution of the upper and lower surfaces, the highest temperature was observed at the leading edge of the lower surface, while the lowest temperature was recorded in the middle of the upper surface. Furthermore, the temperature of the upper surface was found to be higher than that of the lower surface.

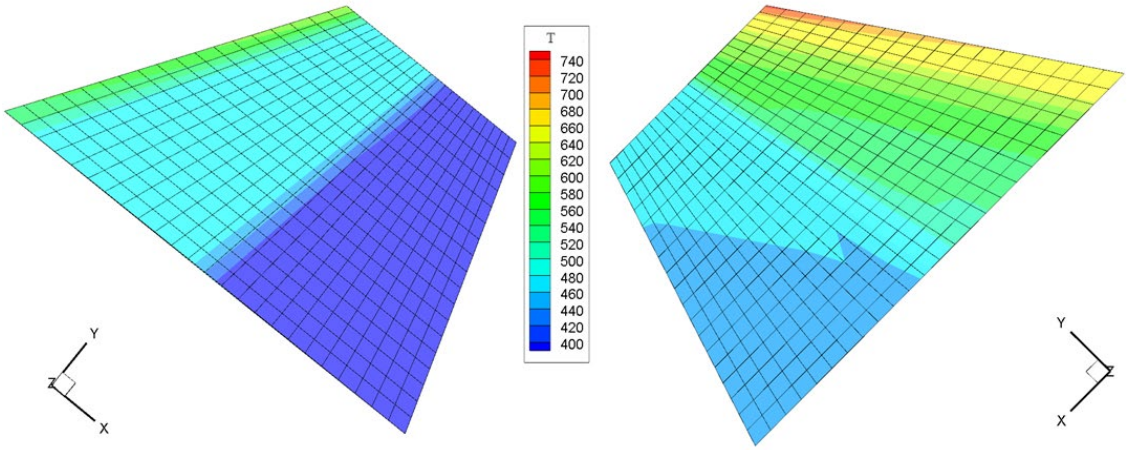

Fig. 7 Temperature distribution of the upper and lower surfaces (t=2 s)

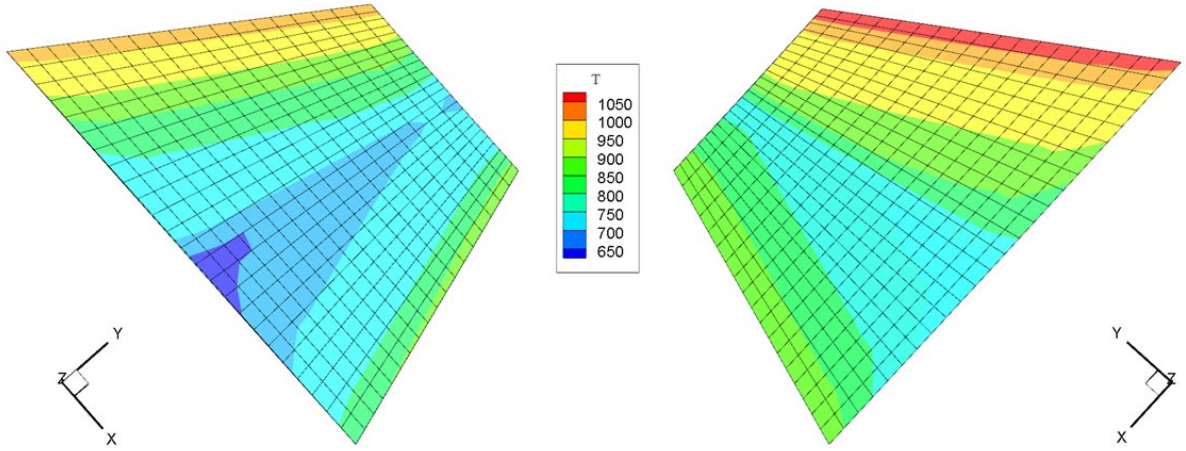

Fig. 8 Temperature distribution of the upper and lower surfaces (t=200 s)

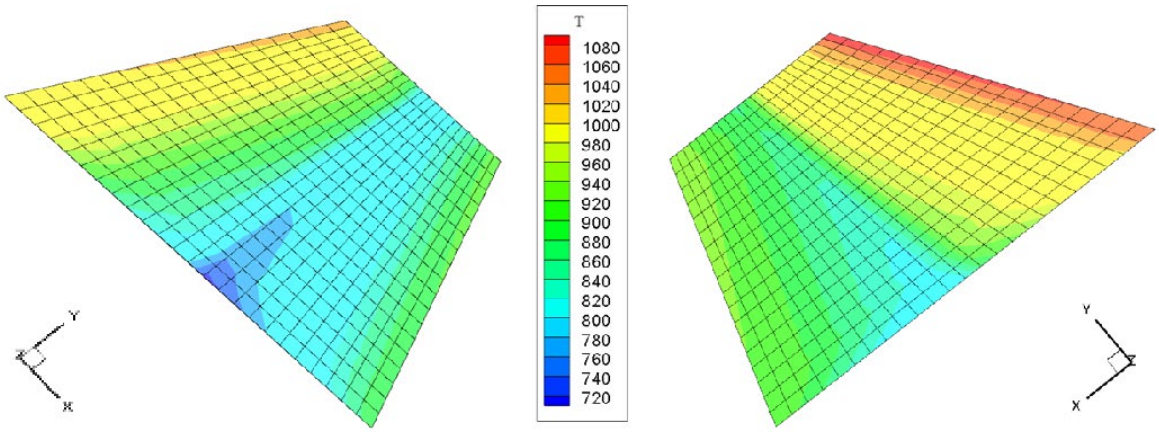

Fig. 9 Temperature distribution of the upper and lower surfaces (t=400 s)

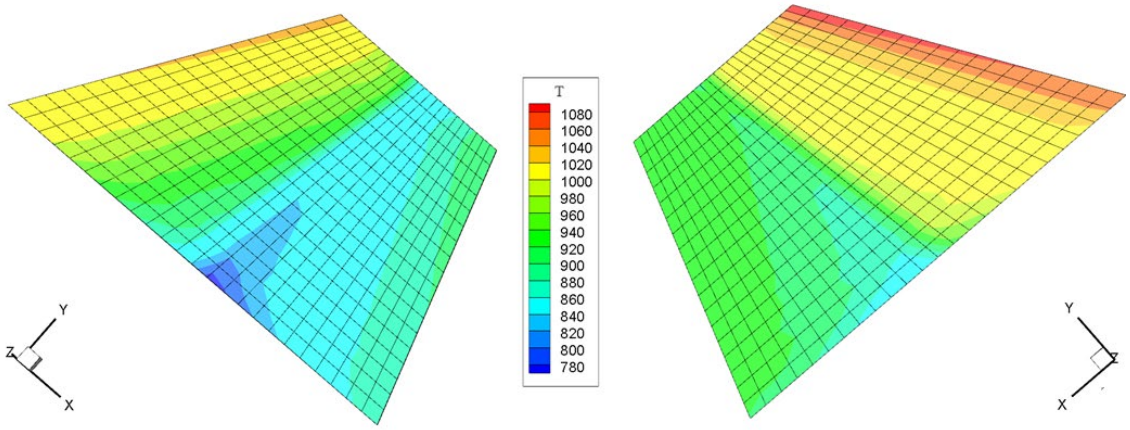

Fig. 10 Temperature distribution of the upper and lower surfaces (t=600 s)

3.3 Flutter characteristics

A thermal flutter analysis was conducted based on the variation of the stiffness matrix obtained from the temperature field of the structure, as determined by the static aerothermoelastic analysis. The temporal variation of flutter speed is illustrated in Fig. 11. It can be observed that the flutter speed is gradually decreasing over time, from 1665 m/s in the absence of thermal load to 1444 m/s at the conclusion, representing a reduction of 13.27%. This indicates that thermal load exerts a significant influence on the stability of the FGM-containing hypersonic wing. Furthermore, it is noteworthy that the flutter speed versus time relationship can be attributed to two distinct curves and the flutter speed jumps abruptly on the two curves as time advances.

In order to ascertain the cause of the abrupt change in the flutter speed of the FGM structure over time, this section presents a detailed comparison of the temperature distribution, thermal stresses, modes, and flutter characteristics of this hypersonic wing before and after the sudden change at t=180s and t=200s, as shown in Fig. 8 and Fig. 12-Fig. 18.

It can be observed that the distribution trends of temperature and thermal stresses at t=180s and t=200s are very close to each other. The minimum temperature inside the structure at t=200s is

slightly higher, the maximum stress is slightly smaller and the minimum stress is slightly larger. It can also be observed that the thermal stresses at the skin are smaller and change more smoothly due to the continuous variation of the FGM properties in the thickness direction.

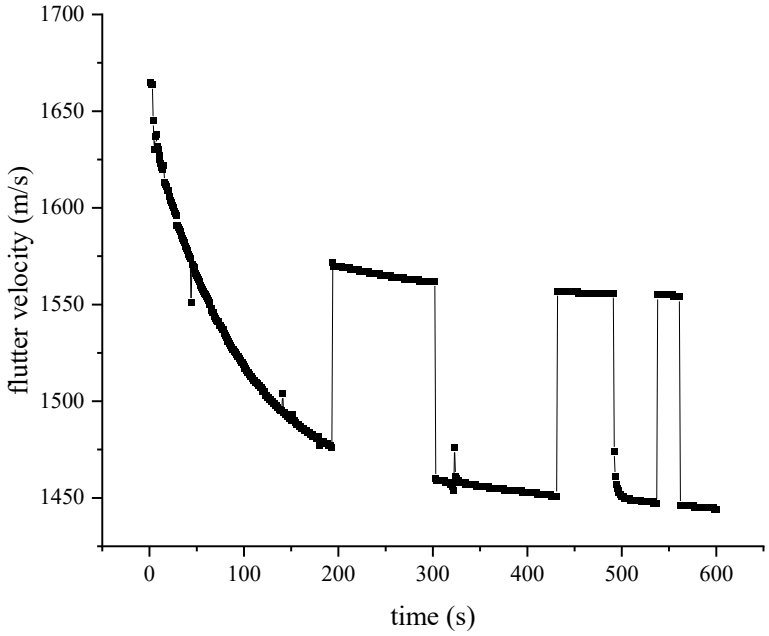

Fig. 11 The variation of flutter speed over time

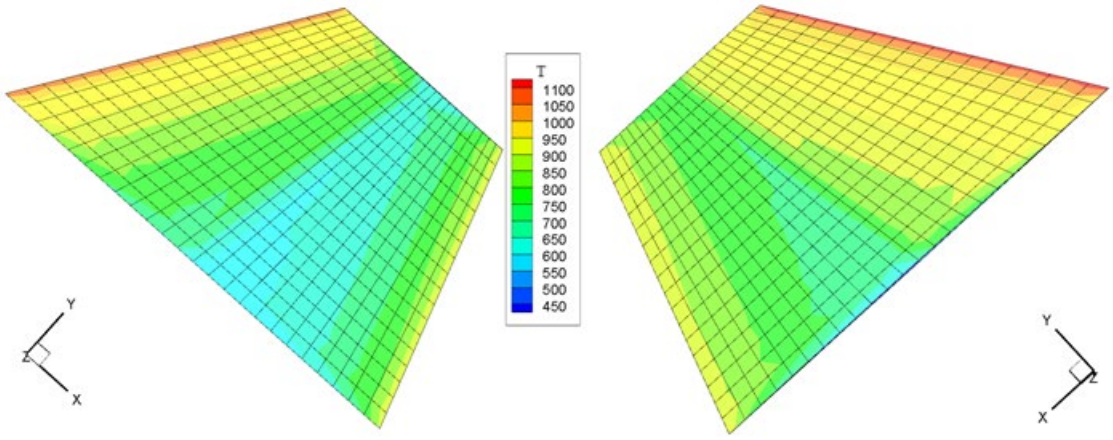

Fig. 12 Temperature distribution of the upper and lower surfaces (t=180 s)

Fig. 15 and Fig. 16 illustrate that the flutter of this FGM-containing hypersonic wing is a coupling of the first two modes. The curve corresponding to the first-order mode on the V-*g* curve crosses the *x*-axis from the bottom to the top, indicating that the required damping for equilibrium is transformed to be positive, i.e., the flutter occurs. Furthermore, the frequencies corresponding to the first two modes on the V-*f* curve are coincident. The curves at 180s and 200s are similar to

each other, yet there is a discrepancy in the flutter speed, which is 1477 m/s and 1570 m/s, respectively.

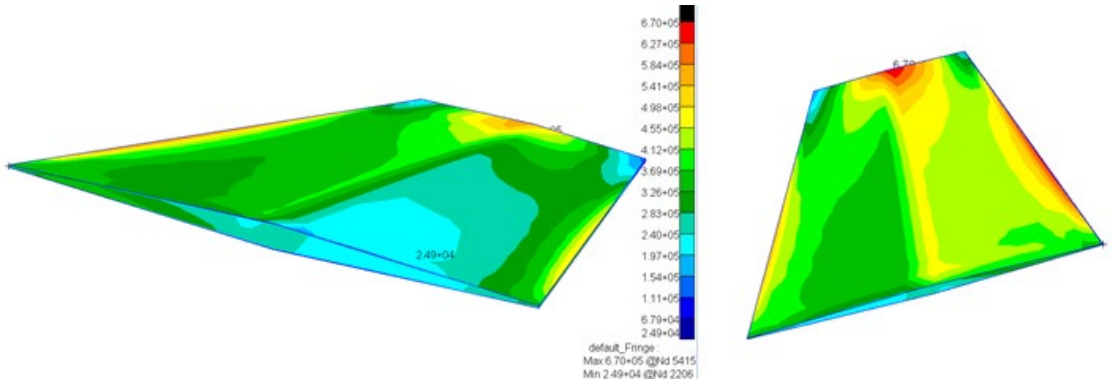

Fig. 13 Thermal stresses of the hypersonic wing at t=180s

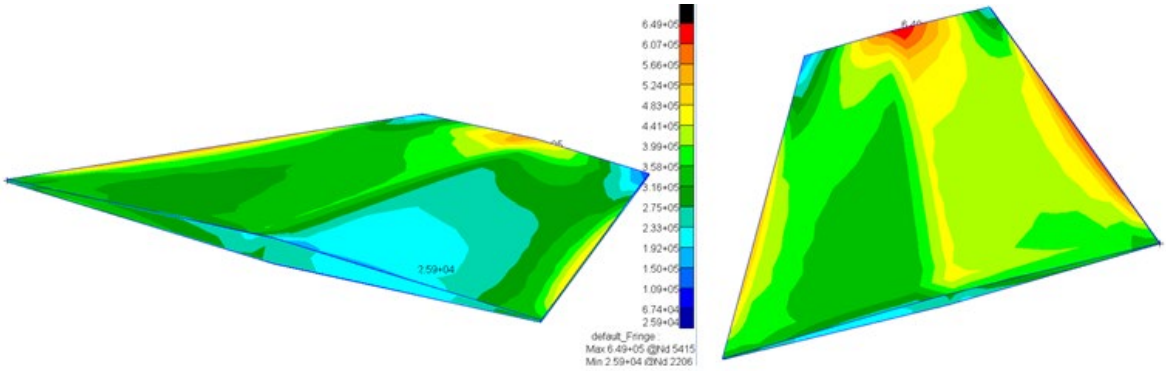

Fig. 14 Thermal stresses of the hypersonic wing at t=200s

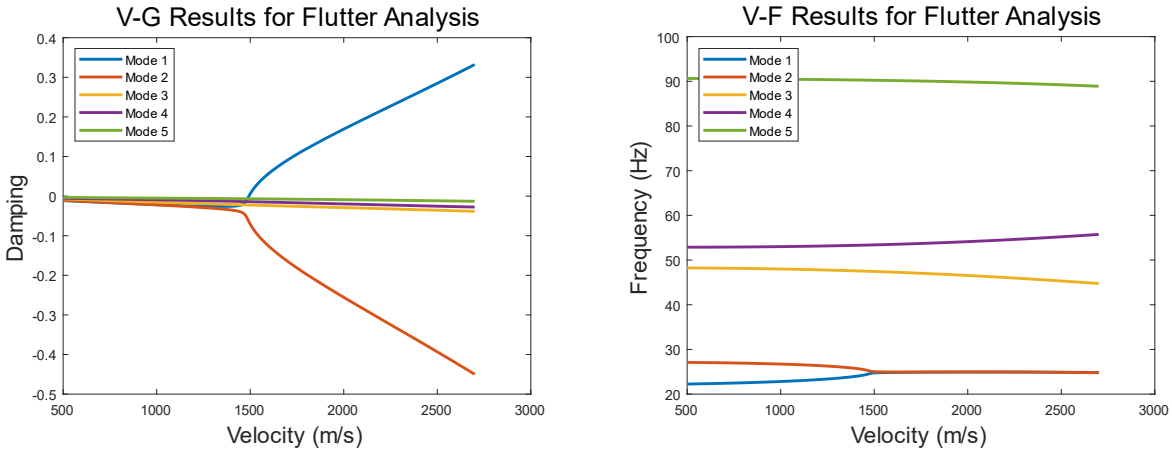

Fig. 15 V-g curves and V-f curves of the hypersonic wing at t=180s

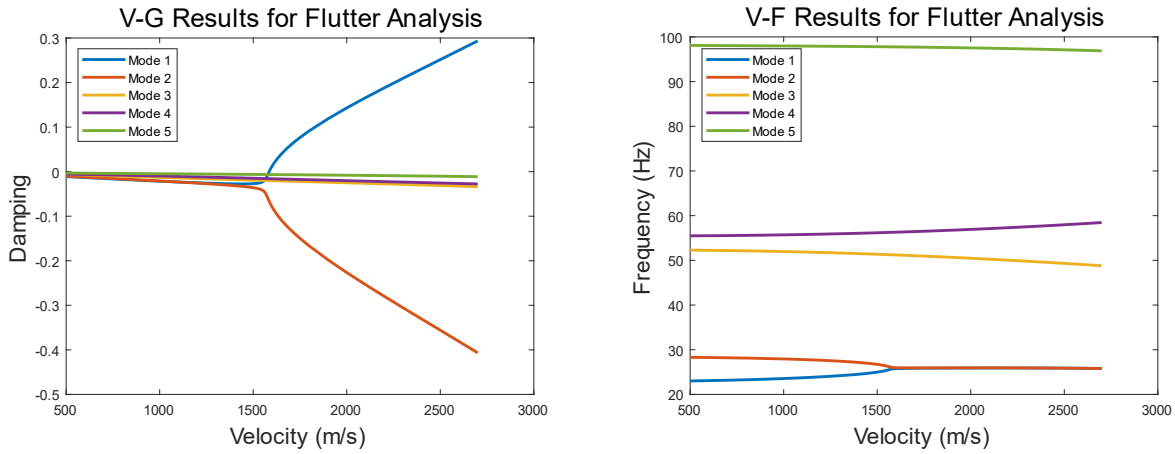

Fig. 16 V-g curves and V-f curves of the hypersonic wing at t=200s

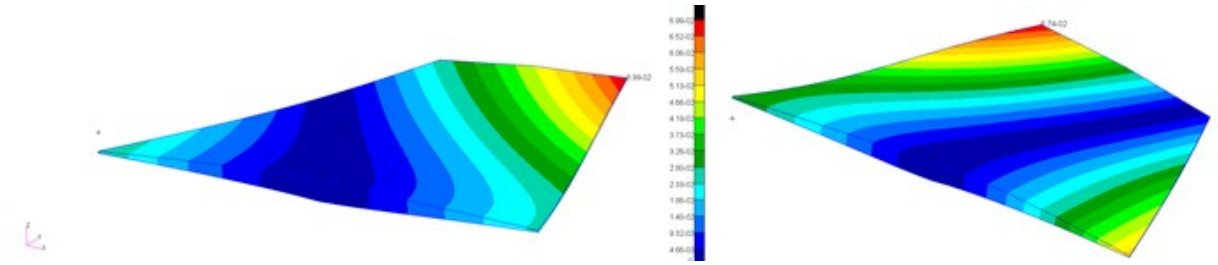

Fig. 17 The first and the second orders of modes of the hypersonic wing at t=180s

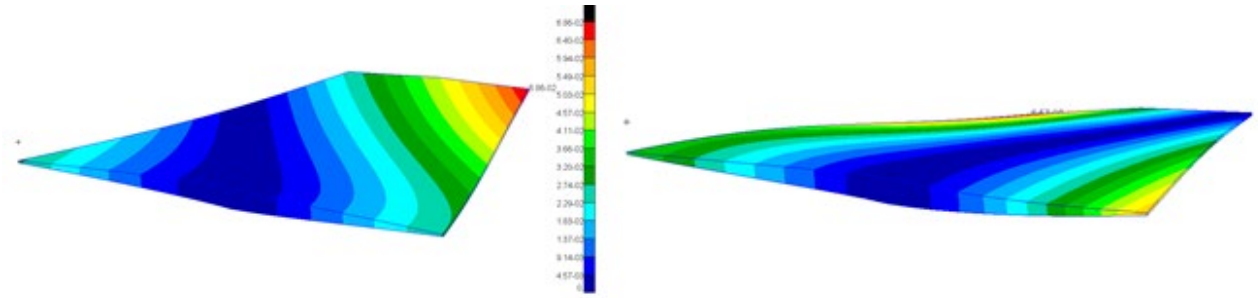

Fig. 18 The first and the second orders of modes of the hypersonic wing at t=200s

The first and second order modes of the heated structure for t=180s and t=200s are illustrated in Fig. 17 and Fig. 18. It can be observed that the mode shape of the first-order is almost the same at both moments, while the mode shape of the second-order mode is completely opposite. After examining several other moments, it was found that the second-order modes at the moments of the lower curve in Fig. 11 are all positively torsional along the diagonal, while the second-order modes at the moments of the upper curve are all negatively torsional along the diagonal. The frequencies of the first two orders of the modes are 22.115 Hz and 27.2 Hz at t=180s, and the first two modal frequencies are 22.85 Hz and 28.392 Hz at t=200s. In contrast, the frequency is lower and the maximum component is larger at t=180s.

Therefore, the reason that the relationship between the flutter speed of the FGM structure over time will produce an abrupt change in the two curves is not due to a change in the coupling mode orders. Both of these curves represent the coupling of the first two orders of modes. Rather, it is due to the properties of the FGM structure that are sensitive to the thermal load. As time progresses, heat is gradually transferred to the interior of the structure, resulting in a change in the distribution of the structural temperature field. This, in turn, affects the structural properties, causing a shift from positive torsion to negative torsion in the second-order modes. This is accompanied by a significant increase in flutter speed. Once the structural temperature field has been altered again, the structural properties revert to their previous state, resulting in a shift of the second-order modes back to positive torsion. The mode transitions to positive torsion, and the flutter speed reverts to the preceding curve.

4 CONCLUSIONS

This paper proposes an integrated static/dynamic aerothermoelastic analysis framework for functionally graded structures in hypersonic vehicles with a two-way coupling strategy. This framework enables the simultaneous analysis of the static aerothermoelastic response of the FGM structure and the thermal flutter during the flight. It also allows for the rapid and comprehensive acquisition of the aerothermoelastic characteristics, which serves as a foundation for the design of the FGM structure in hypersonic vehicles.

Furthermore, this paper identifies a phenomenon that the flutter speed of FGM structures in hypersonic vehicles undergoes an abrupt change with time advancement due to the heat load sensitivity. The reason for this phenomenon is that the internal temperature field of the FGM structure changes over time, which leads to a sudden change in the second-order mode shapes, and subsequently to a sudden change in the flutter speed.

REFERENCES

[1] McNamara JJ, Friedmann PP. Aeroelastic and Aerothermoelastic Analysis in Hypersonic Flow: Past, Present, and Future. *Aiaa Journal*. 2011;*49*:1089-122.

[2] Schoneman J. Aeroelastic Verification of a Dynamic Aerothermoelastic Analysis Framework. AIAA Scitech 2019 Forum2019.

[3] Quan E, Xu M, Yao W, Cheng X. Analysis of the post-flutter aerothermoelastic characteristics of hypersonic skin panels using a CFD-based approach. *Aerospace Science and Technology*. 2021;*118*.

[4] Vargas Venegas CA, Huang D. Physics-Infused Reduced Order Modeling of Hypersonic Aerothermal Loads for Aerothermoelastic Analysis. AIAA SCITECH 2022 Forum2022.

[5] Xie D, Dong B, Jing X. Effect of thermal protection system size on aerothermoelastic stability of the hypersonic panel. *Aerospace Science and Technology*. 2020;*106*.

[6] Vidanović N, Rašuo B, Kastratović G, Grbović A, Puharić M, Maksimović K. Multidisciplinary Shape Optimization of Missile Fin Configuration Subject to Aerodynamic Heating. *Journal of Spacecraft and Rockets*. 2020;*57*:510-27.

[7] Praveen GN, Reddy JN. Nonlinear transient thermoelastic analysis of functionally graded ceramic-metal plates. *International Journal of Solids and Structures*. 1998;*35*:4457-76.

[8] Khalafi V, Fazilati J. Panel flutter analysis of cracked functionally graded plates in yawed supersonic flow with thermal effects. *Applied Mathematical Modelling*. 2022;*101*:259-75.

[9] Xia W, Zhao X, Li D, Shen S. Nonlinear flutter response of pre-heated functionally graded panels. *International Journal of Computational Materials Science and Engineering*. 2018;*07*.

COPYRIGHT STATEMENT